PANIC in the lab: status before commissioning

Bernhard Dorner[*a], Armin Huber[a], M. Concepcion Cárdenas Vazquez[b], Irene Maria Ferro Rodriguez[b], Peter Bizenberger[a], Vianak Naranjo[a], Johana Panduro[a], Ulrich Mall[a], Matthias Alter[a], Richard Mathar[a], Clemens Storz[a], Ralf-Rainer Rohloff[a], Patrick Fopp[a], Werner Laun[a], José Miguel Ibáñez[b], Antonio J. García Segura[b], Víctor Terrón[b], Josef W. Fried[a], Matilde Fernández[b], Julio F. Rodríguez Gómez[b], Klaus Meisenheimer[a]

[a]Max-Planck-Institut für Astronomie, Königstuhl 17, 69117 Heidelberg, Germany; [b]Instituto de Astrofísica de Andalucía-CSIC, Glorieta de la Astronomía 3, E-18080 Granada, Spain

ABSTRACT

PANIC is the new PAnoramic Near-Infrared camera for Calar Alto, a joint project by the MPIA in Heidelberg, Germany, and the IAA in Granada, Spain. It can be operated at the 2.2m or 3.5m CAHA telescopes to observe a field of view of 30'x30' or 15'x15' respectively, with a sampling of 4096x4096 pixels. It is designed for the spectral bands from Z to K, and can be equipped with additional narrow-band filters.

The instrument is close to completion and will be delivered to the observatory in Spain in fall 2014. It is currently in the last stage of assembly, where the optical elements are being aligned, which will be followed by final laboratory tests of the instrument. This paper contains an update of the recent progress and shows results from the optical alignment and detector performance tests.

Keywords: PANIC, CAHA, Infrared, Performance, Optical, Alignment, HAWAII-2RG

1. INTRODUCTION

The origins of the PANIC instrument date back to 2006, where the Scientific Advisory Committee of the Calar Alto Observatory recommended the construction of a wide-field near-infrared imager for the 2.2m telescope. The envisaged science comprises various fields from extragalactic, galactic, star formation, stellar evolution, and solar system areas. Eventually the project was set up as a collaboration between the Max-Planck-Institute for Astronomy in Heidelberg, Germany, and the Instituto de Astrofísica de Andalucía in Granada, Spain.

After the design phase, the PANIC concept has evolved to a compact (<1100mm long) and lightweight (<400kg heavy) near-infrared camera, which can be attached to the 2.2m and 3.5m CAHA telescopes[1]. PANIC is operated at temperatures around 100K, cooled by liquid nitrogen (LN_2).

The instrument will initially be equipped with broadband filters for the bands Z, Y, J, H, Ks, and one narrow-band filter for H_2. It is also possible to add more filters later on for specific observations. The light is recorded by a mosaic of 2x2 Teledyne HAWAII-2RG detectors with 2.5µm cutoff and 2048x2048 pixels each. The optical design incorporates cold field and pupil stops for low thermal background, and provides a field of view of 30'x30' (0.45" pixel sampling) at the 2.2m, or 15'x15' (0.225" pixel sampling) at the 3.5m telescope. An overview of the optical bench with all elements installed can be seen in Figure 1.

The structural layout can be split into a tree structure (Figure 2) starting at the telescope. The cryostat is attached with the Telescope Adapter (TA). Inside, the cold optical bench carries the individual Optics Mounts (OM) 1 and 2. Connected to the OM1 are the Mirror Structure (MS) and the Cold Stop Wheel (CSW) housing. The MS is equipped with three folding mirrors M1, M2, M3 and the Lens Mount 1 (LM1), which holds Lens 1 (L1). The CSW housing carries LM2 with the lenses 2–5 in front of the stop wheel. The second Optics Mount OM2 carries only the Filter Wheel (FW) housing. Attached to it are LM3 with L6–8 in front of the filter wheels, and LM4 with L9 after the filters. At the end, the detector is mounted to the structure.

* dorner@mpia.de, phone: +49 (0)6221 528 388, fax: +49 (0)6221 528 246

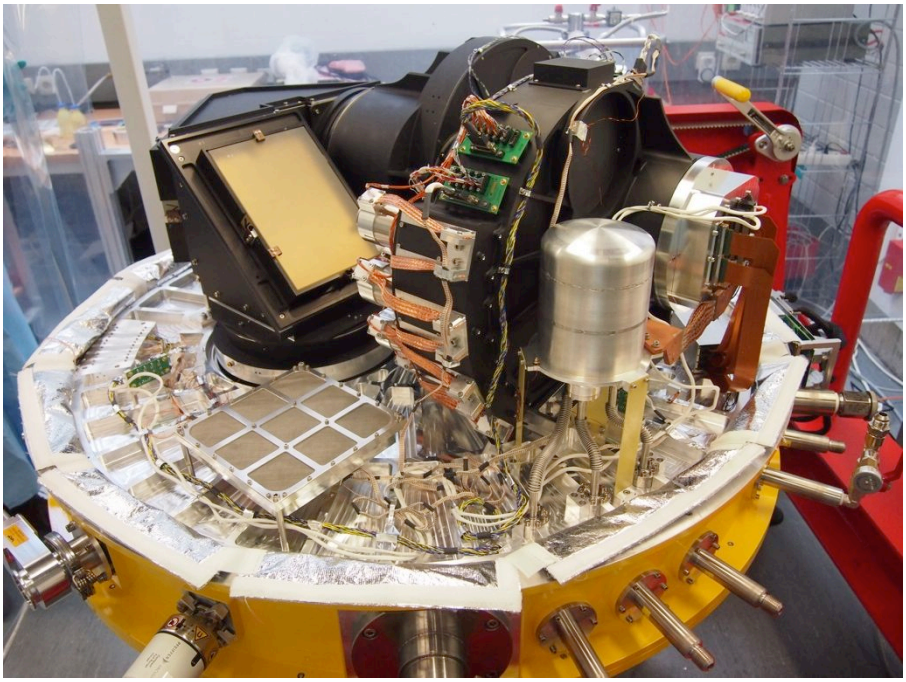

Figure 1: Image of the PANIC optical bench with detectors and optics installed. Light enters from below, and is directed to the main optical elements in the back of the bench. At the telescope, the instrument will be attached upside-down compared to this view.

Significant progress has been made since the last status report in 2012[2]. In late 2013, a test with the full optics and a pinhole mask has been performed to check the influence of flexures in the structures. Although there is clear image motion when tilting the instrument out of Zenith, the impact on the image quality is within tolerances, and the flexures are in the range that can be expected from numerical analysis.

The final integration is now ongoing since mid 2013, and will be completed at the end of summer 2014. Commissioning at the telescope is currently planned at the end of 2014 with general operations starting in the first half of 2015.

2. GENERAL STATUS

2.1 Cryostat performance

Cooldown and warmup of the cryostat have become routine operations after multiple executions for the lab tests, and generally run without problems. It takes about 1 day to reach vacuum conditions, and about 4–5 days to reach working temperatures. The instrument can then be operated without external pumps, while an internal sorption pump with charcoal filling keeps the pressure at about 4×10^{-7}mbar. The maximum holding time for LN_2 is about 40h in the main tank, so refilling has to be done once a day.

The detector has its own LN_2-tank which cools the arrays to about 82K. The temperature can be actively controlled and kept with a stability of about 0.1K. Refilling the detector tank is necessary every two days.

2.2 Mechanisms

PANIC is equipped with two mechanisms: one cold stop wheel and one filter wheel assembly. The former contains two aperture stops for the different pupils at the two telescopes. The latter consists of four separate filter wheels on a common axis in one housing. Each filter wheel has six openings, from which five can hold optical elements or dummies, and one is left open.

The wheels are turned by individual stepper motors via a gearbox. The positions are recorded by hardware switches in the housing, triggered by cams mounted on the wheels. Initialization, driving, and position recognition are tested and work well with the instrument control software. A filter configuration change takes about 20s to execute.

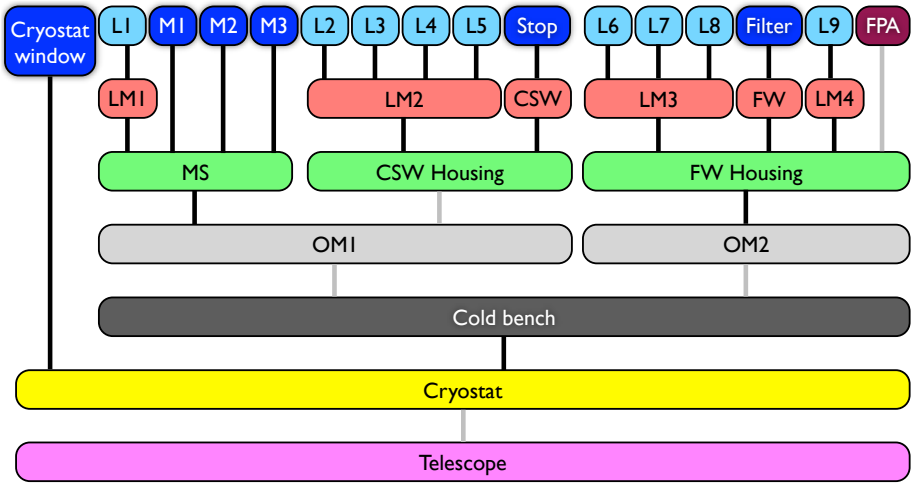

Figure 2: Mechanical structures with nested groups (from bottom up): Telescope, cryostat, cold optical bench, Optics mounts (OMs), Mirror structure (MS) and wheel housings, and Lens mounts (LMs), and individual lenses, mirrors, wheel elements and Focal Plane Array (FPA). The gray interfaces are adjustable with shims and movable pins for the alignment of the opto-mechanical axis and detector focus.

2.3 Electronics

The control electronic equipment of PANIC consists of the wheel drive electronics, the detector temperature control, temperature sensors, one pressure sensor, and warmup heaters. The wheel drives are steered by an MPIA motion controller unit, which includes motor controls and resolver electronics. The detector temperature control is handled by a LakeShore LS332S unit, which includes two temperature measurement and heater control loops. Eight more temperature sensors distributed in the instrument are read by a LakeShore LS218S monitor unit. A Pfeiffer TPG261 full range gauge records the pressure in the cryostat.

An Nport server and an Ethernet switch provide communication with the instrument control computer. The temperature and pressure values are correctly read and stored in the exposure FITS files. The detector temperature control has to be

Figure 3: Control electronics rack. Top row left: Detector thermal control, right: temperature monitor. Center row left: MPIA motion controller, right: Pressure gauge. Bottom: Power supply and fuses. Mounted on the rear side are the Ethernet switch and Nport server.

manually configured at the device, but can be let running during operations. All devices except the warmup power supply are mounted in a small rack (Figure 3), which will be attached below the telescope main mirror cell. The total power consumption of the devices can be up to 150W.

2.4 Software

Several software tools have been developed or adapted to PANIC[3, 4]. The instrument control and readout is handled by the dedicated software GEIRS (GEneric InfraRed camera Software). Minor remaining errors are corrected on the way, general operations are done without problems.

The high level software comprises an Observation Tool (OT) for the design of the observations through Observing Blocks, a Quick Look (QL) for the in-situ data inspection during the observing night, the PANIC Pipeline (PAPI) for the scientific data reduction, and LEMON (Long-tErm Photometric Monitoring) for the data reduction and analysis of time series observations. The interplay of the software packages and the instrument has been successfully tested in the lab. The functionality of the processing pipelines has been verified with data from observations with the camera Omega2000.

3. OPTICAL ELEMENTS

3.1 Lenses

The centering of the lenses in the lens mounts has small tolerances of about 50µm. The lenses have been integrated, centered with micrometer screws, and the residual error has been recorded. After several cryogenic cycles, the errors have been measured again. At warm some of the position residuals are above the stringent requirement. Nevertheless the lenses are stable in their mount and return to the same position as before a cooldown.

3.2 Mirrors

The three folding mirrors have been assembled in the mirror structure and aligned to the correct tilt angles. The mount has been subjected to a tilt test to measure the deformation at different Zenith angles. It was found that the beam direction does not change more than 20” up to a tilt of 60°. The required stability is met with margin.

3.3 Filters

The six science filters have been delivered; their transmission curves in working conditions (100K and converging beam) are shown in Figure 4. The read leaks of all bandpass filters are located at wavelengths beyond 3µm, where the detectors are not sensitive any more. The out-of-band blocking density is at minimum OD=4 in the range 0.3–3µm.

The filters have clear aperture diameters of 11.4cm. Due to problems with the mechanical interface, not all filters have been integrated in the instrument yet. The Ks filter is currently being remade, while the other filters have been retouched.

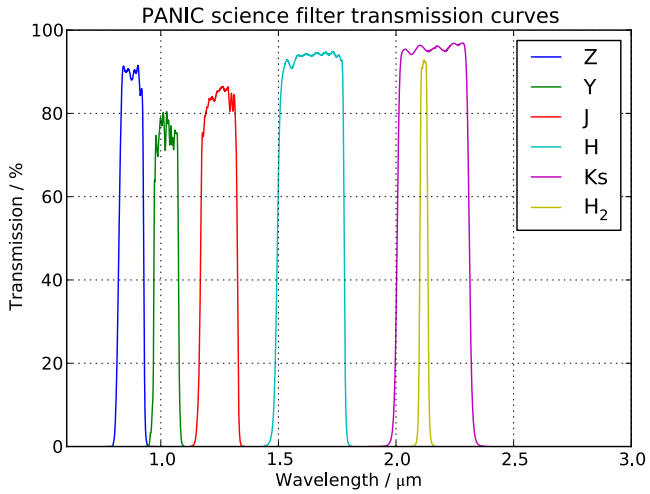

Figure 4: PANIC filter transmission curves in working conditions (100K, cone beam).

Table 1: Planned configuration of the PANIC filter wheels. Science filters are bold. The dummies can be removed and replaced with other filters if necessary.

		Position					
		1	2	3	4	5	6
Wheel	1	**Y**	**H**	PIL	Blank	**J**	Open
	2	**Z**	**Ks**	Blank	**H_2**	dummy	Open
	3	dummy	dummy	Blank	dummy	dummy	Open
	4	dummy	Black	Blank	dummy	dummy	Open

The planned final configuration for the four wheels to be installed in summer 2014 is listed in Table 1. It also includes the Pupil Imager Lens (PIL), one aluminum blank element in each wheel for dark exposures, and eight mass dummies.

The PIL has been optimized for usage with the Ks, therefore this filter and the H_2 will be placed on different wheels. The filters are located in a converging beam, so it is not possible to combine two filters on different wheels due to the change in optical pathlength.

For the ongoing lab cryocycles, only wheel 1 has been populated with optical elements, the others are filled with blanks and dummies. Figure 5 shows wheel 1 from the telescope side after integration in the housing. The glass of the installed Ks was damaged during the cold cycles, but can still be used for the optical tests. An old H filter from the Omega2000 instrument was added and equipped with a diffusor to scatter the light for flatfield exposures.

Figure 5: Image of filter wheel 1 equipped for lab testing. It is populated with filters Ks (top left), H (top right, smaller diameter, from the instrument Omega2000), the PIL (right), and two dummies. The open position is on the left.

4. OPTICAL ALIGNMENT

4.1 Opto-mechanical axis

Tools

The alignment of the large structures (CSW, MS, FW) holding the lens mounts, mirrors, and the FPA was done with a Micro-Alignment Telescope (MAT, Figure 6 right). Its main modes of operation are single pass to measure offsets with a crosshair and micrometer screws, and reflection to measure tilt angles with an internal radial distance reference.

For the first mode, alignment targets can be installed in the instrument at various locations. They consist of two fingers with precisely manufactured edges, providing a reference for the crosshair in the MAT. Two targets are put at the nominal location of the optical axis (Figure 6 left) and serve as the absolute reference. The MAT is placed behind the detector position and aligned to the defined axis with an x/y- and tilt stage. Other targets can be attached at the interfaces

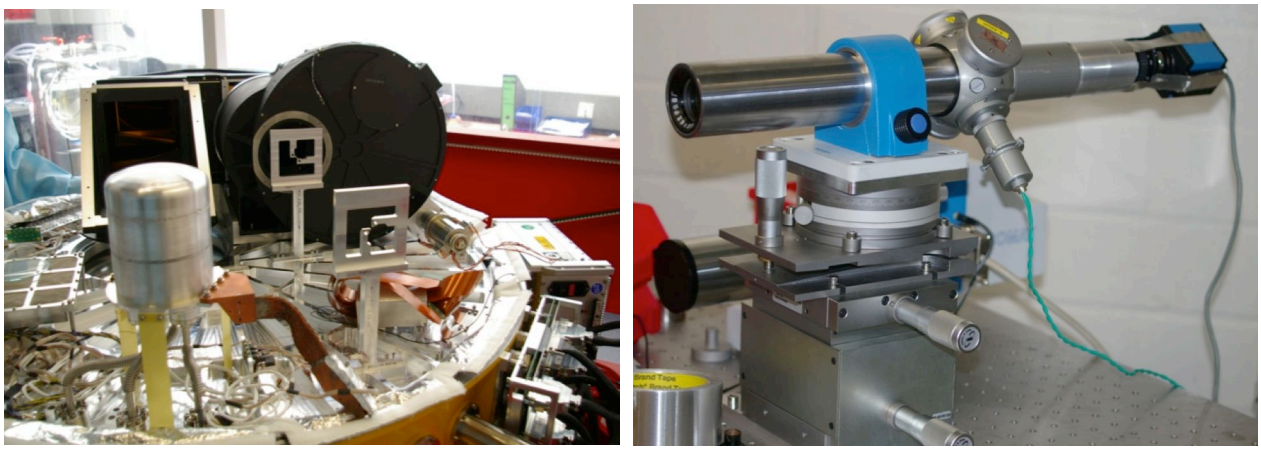

Figure 6: Left: Cold bench with OM1 structures installed and reference targets for the opto-mechanical axis. Right: Micro-Alignment Telescope used in the alignment process.

for the lens mounts and a plate on the telescope adapter in front of the instrument. The target design is such that only little light is blocked and several targets can be homed at in a single configuration.

To measure positions and tilt angles simultaneously, a Reference Mirror (RM) has been manufactured. It has two diamond turned plane and parallel surfaces with a center mark, and can be attached to the interfaces of LM1, LM2, LM3, and with an adapter on top of the telescope adapter. The downside is that it blocks the optical path and obscures targets behind it.

Typical views of the two modes with targets and the RM through the MAT are shown in Figure 7. The left image is the alignment of the crosshair to the target edges. The center image is the measurement of the position offset with the RM center mark. The right image is the measurement of the RM surface tilt. The position of the crosshair in the reference circles can be converted to the surface tilt once the distance between MAT and RM is known.

The accuracy of a single position measurements is about ±30µm, the tilt can be measured with an accuracy of about ±0.2'. In addition, the measurements are very sensitive to the orientation of the MAT set by the reference targets. This step obviously has the same accuracy of a measurement, and leads to variations in the MAT axis position. Therefore, position data taken at long distances can have large errors. Since the individual alignment tolerances can be as small as ±50µm and ±1', multiple measurements (done with individual MAT alignments) are necessary to achieve a sufficient accuracy.

Methods

Not all the structures can be adjusted independently. As the scheme in Figure 2 shows, a movement of the OM1

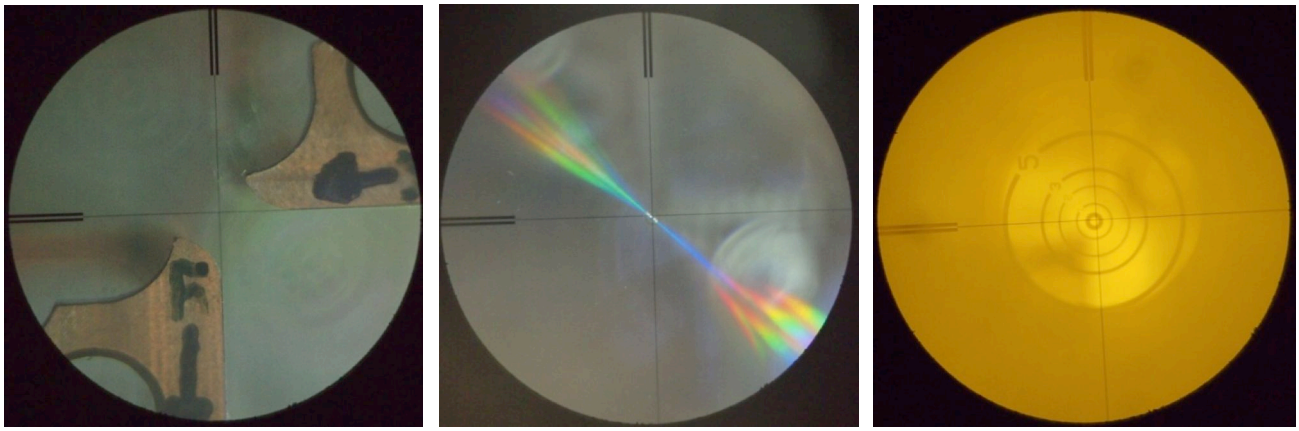

Figure 7: Views through the MAT: Left: Alignment targets, center: the RM for position data, right: the RM for tilt data.

influences all optical elements in this group. However, only some interfaces are suitable for precision alignment. In particular there is no possibility to adjust positions or angles between lens mounts and their holding structure. Therefore only four interfaces were used in the axis alignment, and only five mounts have been measured. The relative positions of others on the same structure are kept in range by small manufacturing tolerances.

The goal of the alignment was to bring the optical elements in x/y-position and tilt to a common axis defined on the optical bench by the two reference targets. An alignment to the telescope axis can then be done at the telescope adapter interface (as long as the offset stays within the allowed range). There are significant changes in the positions between having the optical bench up (lab working position) and down (as during operation), and between warm and cold conditions. Therefore the measurements were taken at cryogenic temperatures and in Zenith position, while the corrections were performed at warm and with the bench up. As the tilt angle could only be measured with the RM at a single interface, multiple cryocycles were necessary to get all structures aligned.

The first step was to bring LM1 in position. The interface between OM1 and the MS turned out to be little repeatable, so LM1 could only be influenced by moving OM1 as a whole. Taking into account that the CSW-OM1 interface is only easy to move in certain directions, a proper alignment of LM1 was found by shimming and moving OM1. Besides, the mirror holder of the plane fold mirror M1 was shimmed to achieve a common position. Attaching the RM to LM2, this interface was adjusted next by shimming the CSW on OM1. Since the housing position is defined by mechanical stops, certain movements required removing material from the structures.

In all runs, LM3 and LM4 have been equipped with their targets, and the tilt of LM3 was assumed as the tilt of the direction between LM3 and LM4. This assumption is allowed since they sit on opposing sides of the CSW housing, which is manufactured to accuracies below the tilt tolerances. Besides, the lenses are more sensitive to position offsets than tilts, so bringing both interfaces to a position close to the axis is more important than their actual local tilt. The adjustment of LM3 and LM4 was done by moving and shimming OM2 on the optical bench.

Finally, the attachment of the instrument to the telescope was pre-aligned by mounting the MAT on top of the telescope adapter. The MAT was centered orthogonally along the expected optical axis of the telescope. The weight of PANIC will deform the telescope adapter when hanging at the Cassegrain focus; this effect was derived with an FEM model. With the RM on LM2, it was possible to calculate the required measurement with the MAT to be on a common axis with the optical bench. At the end, the plate on top of the TA was moved and tilted by remachining the shims at the interface.

Results

For verification, the positions have finally been measured several times with only targets installed. The angles of LM1 and LM2 have been taken from the last measurements with the RM. The results are listed in Table 2, and positions are plotted in Figure 8. The errors are the scatter from the 5–8 individual measurements. They are equally large for the tilt angles, but increase strongly with distance from the MAT for position data. The initial alignment to the reference targets is very difficult, and small differences in angles there lead to large position changes at longer distances.

It is not important to meet the design axis of the instrument, but to place the elements on a common axis. Therefore the

Table 2: Data and residuals of the opto-mechanical axis alignment at different interfaces in position and tilt angles. The tolerances are typically 100–50µm and 1–1.5'. Tilts of the TA and LM4 have not been measured.

		TA		LM1		LM2		LM3		LM4	
		X	**Y**	**X**	**Y**	**X**	**Y**	**X**	**Y**	**X**	**Y**
Position / µm	**Measured**	66	802	42	-6	-18	510	24	512	0	550
	Error	100	87	37	71	15	29	20	13	7	19
	Residual	17	398	8	-451	-30	6	19	-12	3	6
Tilt / arcmin		**X**	**Y**	**X**	**Y**	**X**	**Y**	**X**	**Y**	**X**	**Y**
	Measured			0.18	-0.04	-0.56	-0.28	-0.44	-0.28		
	Error			0.03	0.09	0.09	0.22	0.10	0.23		
	Residual			0.42	0.05	-0.32	-0.19	-0.20	-0.19		

residuals are given with respect to a least-squares fit of the positions of LM1–LM4 in x, and LM2–LM4 in y. Especially in y, the final axis is therefore about 0.5mm above the design.

The position residuals are very small in x in all locations. In y, only LM2–4 meet the specifications, LM1 is 0.45mm off, similar to the TA. However, the effect of the decenter of L1 has been simulated and found to be negligible if the other lenses are so close to their required positions. The offset of the TA is not critical. Eventually it has to be adjusted at the telescope, and is small enough to allow this correction with the existing hardware pieces. The tilts of the TA and LM4 have not been measured, but are not critical. The tilt with respect to the telescope has a large tolerance of several arcminutes and can still be corrected with shims, while the angle of LM4 is limited by the manufacturing tolerances of the CSW housing. The tilt of the detector is adjusted in a separate step (see subsection 4.3). The alignment of the structures therefore meets the requirements.

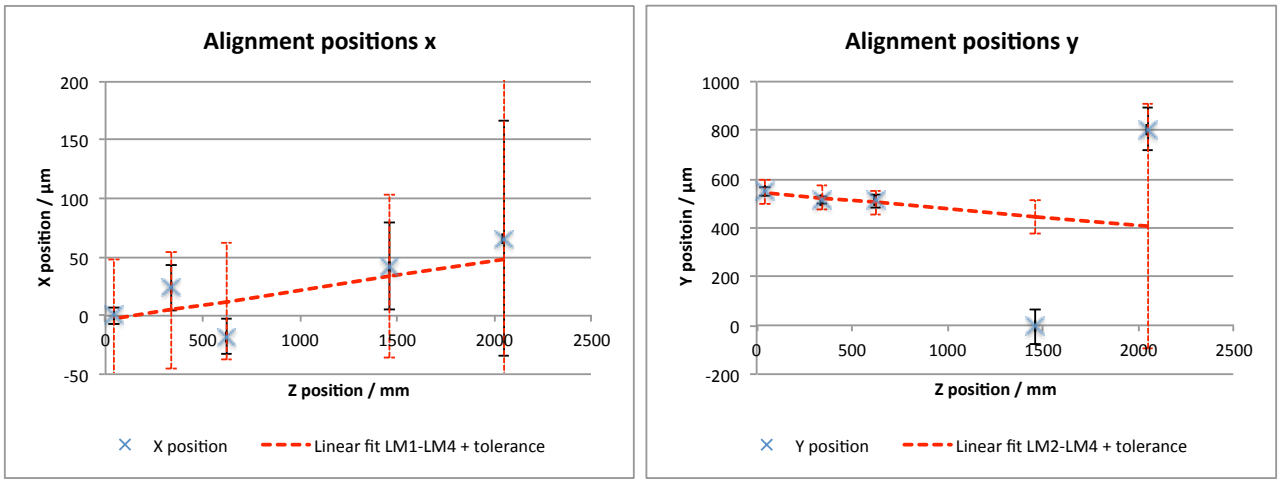

Figure 8: Positions on the opto-mechanical axis after alignment and linear fit in x- and y-direction. The points are (left to right): LM4, LM3, LM2, LM1, telescope adapter. The lens mount tolerances allowed are 100–50µm. The measurement errors increase with distance to the MAT located behind LM4. LM1 is far off in y, but the effect on the optical quality is negligible. The offsets of the TA are small enough that they can be corrected at the telescope, where the tolerances are very large.

4.2 Lens z-positions

Adjusting the positions of the LM interfaces also fixed some distances along the optical path, which have an impact on the image quality. Therefore, the mounts of the lenses L3 and L8 allow the change of their z-position for compensation. The thicknesses of their z-compensators have been optimized with a Zemax model including the as-built data of the lenses and distances in the instrument, and the lenses have been integrated in the barrels with adapted pieces.

4.3 Detector focus and image quality

The last step in the alignment sequence is the adjustment of the detector focus and tilt. Since PANIC is not equipped with a focus mechanism, the array positions have to be aligned at cold with the conjugate of the nominal telescope focal plane at the entrance of the instrument. For this purpose a focal mask (Figure 9 left) can be installed instead of the field stop right after L1. Multiple pinholes of 0.3mm diameter are drilled into the disk. Their size corresponds to about 8 pixels on the detector. The telescope focal surface is curved and intersects the plane mask at a certain radius marked with a ring of pinholes.

To allow the determination of the best focus, pinhole inserts are mounted in each quadrant. They contain an array of 9 or 12 holes at distances of 1 and 2mm from the insert bottom side. This way, four grids of holes are available at distances –2, –1, +1, and +2mm from the mask surface and produce differently defocused images. The inserts are mounted around the intersection with the telescope focal sphere. Due to the curvature, the average distances of the grids are z = –2.46, –0.83, +0.78, +2.37mm from the actual focus position. One example of the pinhole images is shown in Figure 9 right. The four pinhole grids are clearly differently focused.

The sizes of the pinhole images are measured by the FWHM of a fitted Gaussian. Taking the average of each grid for one focal distance and three close-by pinholes at the z=0 position, a parabola is fitted through the five points, as shown in

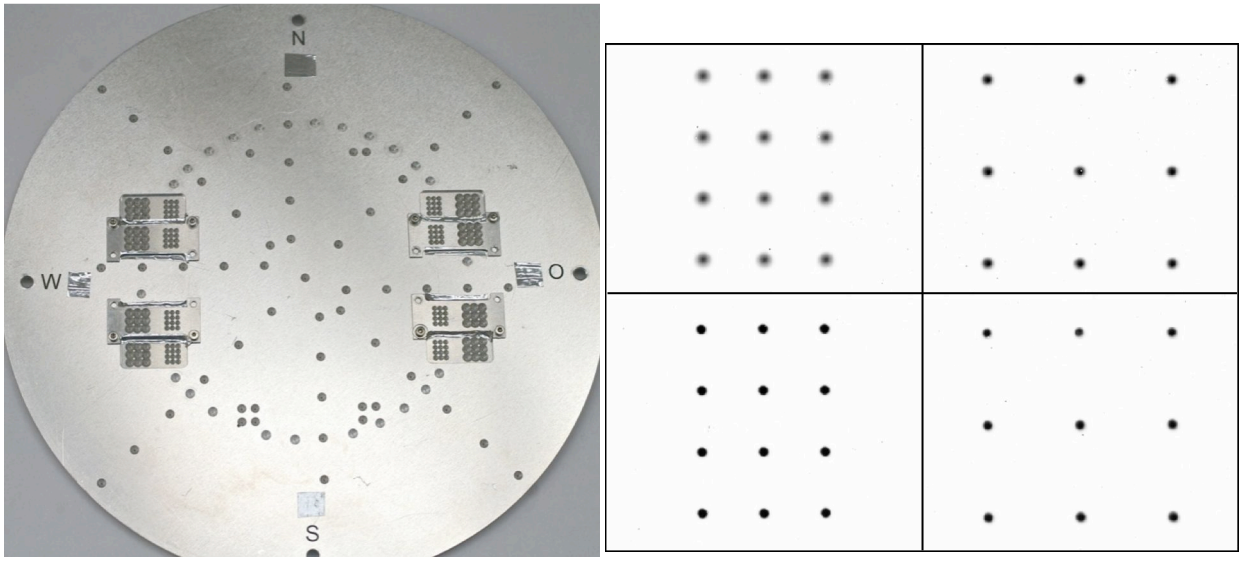

Figure 9: Left: Focal mask placed at the instrument entrance. The intersection with the telescope focal sphere is at the location of the pinhole ring about halfway from the center. In each quadrant there are four additional pinhole grids mounted at different focus distances. Right: Test image of pinholes at approximate focal distances in linear scale, zoom on single grids: z = –2.4mm (top left), –0.8mm (top right), 0.8mm (bottom left, sharpest image), 2.3mm (bottom right).

Figure 10. The minimum then denotes the local position of the conjugated detector plane at the instrument entrance. By converting the offset to the detector focal plane, it is possible to derive the correction necessary to bring the mask position z=0 into focus. This correction is then applied to the distance ring placed at the FPA mechanical interface. The alignment process is currently ongoing and will be finished around end of June 2014.

Eventually, the image quality of the optics will be verified with a star simulator. This device projects an optical fiber to the telescope focal plane with a spot size smaller than the instrument PSF. It will probe various locations in the field, and the spot shape will be checked for anomalies. If particular asymmetrical aberrations can be traced back to a certain lens, it will be possible to correct lateral decenters if necessary.

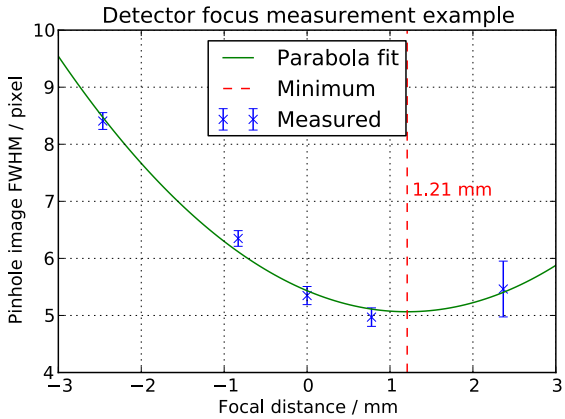

Figure 10: Example of pinhole sizes in one quadrant from the first detector focus adjustment. The minimum at 1.21mm indicates that the FPA is not yet at the correct position.

5. DETECTOR PERFORMANCE

5.1 Setup and data

The optimization of the detector and readout electronic parameters[2, 5] with the final science-grade (SG) arrays has been going on until mid 2013. The detectors have been integrated in the instrument at various occasions, and are now

constantly mounted for the optical tests. In each cryogenic cycle, standard characterization data are recorded along with the optical test exposures to monitor the FPA status. The default data consists of:

- Flatfield exposures with varying integration time (shortest to 150% average saturation),
- Dark exposures with varying integration time (shortest to about 30min),
- Numerous dark exposures with shortest possible integration time.

Each data type is recorded with the readout modes rrr-mpia and lir[6], which are the standard modes that will be offered for observations. The default output of GEIRS is a double-correlated image (difference read – reset), but to analyze some features, the single frames are saved in addition. Besides, some up-the-ramp cubes are recorded to investigate particular effects.

A standard desk lamp mounted on top of the telescope adapter provides the external illumination in the lab. Its brightness can be adjusted with a voltage transformer, and by putting bulbs of different power. Since the focal mask is placed at the entrance of the instrument during the ongoing optical tests, it is not possible to create a flat illumination of the detectors.

The best makeshift is to use the H-filter with the diffusor to remove the imprint of the pinholes, and illuminate the entrance with high power. Unlike the field stop, the focal mask lets some light pass at the edges of the field. With enough intensity, the straylight illuminates the detector mosaic with large-scale variations of 15%. This is sufficient for health monitoring and correcting pixel-to-pixel variations. A proper flatfield for characterization will be taken without the focal mask at a later stage.

5.2 Results

The results shown in Table 3 originate from the detector focus test runs in April and May 2014. The presented values are derived from median-averaged data taken in rrr-mpia read mode or srr sample-up-the-ramp cubes.

Gain

The detector gain has been derived by the photon transfer curve method from the flatfield data. The detector fullwell capacity of about 220,000 electrons can be fully mapped to the ADC range of about 60,000ADU. The total dynamic range can be exploited within the limits of having small enough deviation from a linear response.

Table 3: Overview of performance data of the four arrays. Gain, saturation and read noise are similar to the manufacturer test data. The median dark current of SG4 is severely influenced by hot pixel degradation as apparent in the pixel status fractions.

Data		**SG1**	**SG2**	**SG3**	**SG4**
Gain / e–/ADU		4.45	4.69	4.82	5.96
CDS saturation limit	ADU	50376	48994	46903	42454
	e–	224173	229782	226072	253026
CDS Read noise / e–		15.1±2.9	17.3±3.5	19.0±3.8	21.4±4.6
Dark current / e–/s	Median	0.816	0.838	1.391	17.64
	Mode	0.842	0.602	0.827	2.285
Pixel status fractions / %	Super hot (Dark rate >25,000e–/s)	0.06	0.27	1.19	7.88
	Hot (Dark rate >2,500e–/s)	0.14	0.82	2.87	16.97
	Low QE (signal <15% of median)	0.02	0.28	0.17	0.13

Saturation limit and linearity

The maximum number of counts per pixel was determined with long flatfield images. To compensate the spatial variation of the illumination, the exposure time was set up to 150% of the average time until saturation. The median of each array was observed as a function of the integration time, and becomes constant at the end. These values of the longest exposure are given in Table 3. They are sufficiently large with numbers in the range of 42,000–50,000ADU. The value of SG4 seems small, but is compensated by the larger gain.

Since there is no non-linearity correction available in the software up to now, a rough upper limit for valid data in the lab tests has been set at 90% of the saturation level of each individual pixel. However, it will be necessary to add such a correction for scientific data. Preliminary analysis showed that the behavior is only linear within 1% error in the range of 5–30% of saturation.

Read noise

The mean readout noise has been calculated as the standard deviation in each pixel from 20 dark exposures with minimal integration time. The pixel-to-pixel histogram was fitted with a Gaussian distribution, whose mean and sigma are given in the table. The CDS values are about 18e–, which is marginally larger than the values from the characterization at Teledyne, but well within the allowed range for the instrument. The value of SG4 is increased by the shot noise of many pixels with high dark current.

Dark current

The dark current has been measured with srr up-the-ramp exposures of 150s duration with 2.5s frame time. The first frame has been subtracted, and the ramps were fitted with lines excluding saturated values. The median dark current is in the range of 0.8e–/s for SG1+2, slightly elevated for SG3, and strongly distorted for SG4. This array suffers from hot pixel degradation typical for this detector generation[7, 8]. The modal dark current (most frequent value in the histogram) is about 0.8e–/s for SG1–3, and already 2.3e–/s for SG4.

Unfortunately the dark current ramps become non-linear above values of about 1–2e–/s due to field enhanced emission. Therefore a simple linear fit to slopes gives distorted values at high rates, and is not usable for science data reduction. At the telescope, a non-linear modeling or dark images with exposure times equal to science data will be required.

Pixel status

The pixel status and operability has been checked with dark and flatfield images. The instrument will normally be sky-background limited, therefore a mildly elevated dark current is no issue. However, with the strong degradation of SG4 it was necessary to introduce limits for the tolerable dark range.

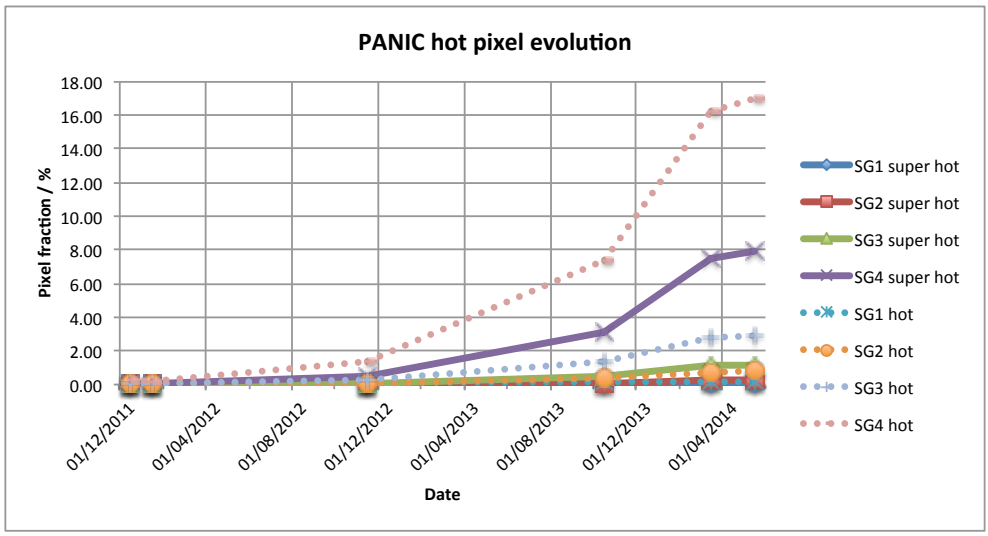

Figure 11: Hot pixel fraction of the PANIC detectors over time. Super hot rates are >25,000e–/s, hot rates are >2,500e–/s. There is a massive increase in SG4 after 2012 and it has become unusable due to this degradation. Levels in SG3 started to rise, but the degradation has slowed down after keeping the arrays mostly at cold in the instrument.

Clearly unusable are “super-hot” pixels with >25,000e–/s, which means saturation in less than 10s. Any signal on top leads to imminent saturation or is not resolvable in the shot noise. Hot pixels have dark currents >2,500e–/s. Depending on the sky brightness, they may become unusable. For the K-band, the signal is at worst comparable to the one expected from the sky background, but data of shorter wavelength bands will be degraded.

The pixel fractions have been calculated from the dark rate derived from short dark exposures. While SG1–2 are in good conditions and SG3 has only a larger amount of warm pixels, SG4 has become unusable for science. 7.9% of its pixels are completely inoperable and further 9.1% critical.

Pixels with low QE can be found from flatfield data. They are characterized by having values <15% of the median of an image with about 50% saturation. The fractions are below 0.3% for all detectors.

5.3 Hot pixel evolution

To track the evolution of the detector characteristics, short dark data taken in the various readout optimization runs has been analyzed the same way as above. The fractions of super-hot and hot pixels are plotted in Figure 11. The hot pixel rates have continuously risen since the first tests. In particular the array SG4 has reached a scientifically unusable state. The degradation was favored by the storage at ambient conditions. The decay has slowed down in the beginning of 2014, where the detectors have been installed in the instrument, and kept at cryogenic conditions most of the time.

There are plans to exchange SG4 with a new array once the instrument has been commissioned at the observatory. Until then, one quadrant will be unusable for science observations. Although SG3 shows signs of starting degradation, its rate of decay is much lower and it will be slowed down even more now that the instrument is mostly kept cold. Nevertheless, the general increase in dark current in all detectors brings more difficulties in the observation planning and data processing.

6. CONCLUSION

The PANIC instrument has made significant progress during the last year. The opto-mechanical axis alignment has been completed, and the focus is currently being adjusted, followed by be the evaluation of the image quality. The mechanical and electrical equipment is working well. The detector readout has been optimized, and may only need some fine-tuning. The control and data processing software is very mature and debugged progressively. The lab activities at MPIA are expected to finish at the end of summer 2014.

After shipment to CAHA, PANIC will undergo a final lab acceptance test and installation at the telescope. The commissioning is currently in preparation. After successful installation at the observatory, one degraded detector will likely be replaced to fully exploit the large field of view.

REFERENCES

[1] Fried, J.W., Baumeister, H., Huber, A., Laun, W., Rohloff, R., and Cárdenas, M.C., “Opto-mechanical design of PANIC”, Proc. SPIE 7735, 77353V (2010)

[2] Fried, J.W, Storz C., Mall U., Naranjo V., Bizenberger P., and Cárdenas Vázquez M.C., “Laboratory performance tests of PANIC, the panoramic NIR imager for Calar Alto”, Proc. SPIE 8446, 84462Q (2012)

[3] Ibáñez Mengual, J.M., Fernández, M., Rodríguez Gómez, J. R., García Segura, A. J., and Storz, C., “The PANIC software system”, Proc. SPIE 7740, 77402E (2010)

[4] Ibáñez Mengual, J.M, García A.J, Storz C., Fried J. W., Fernández M., and Rodríguez J. F., “Advanced PANIC quick- look tool using Python”, Proc. SPIE 8451, 84511E (2012)

[5] Naranjo, V., Mall, U., Ramos, J.R., Storz, C., Wagner, K., Alter, M., Baumeister, H., Bizenberger, P., Cárdenas, M.C., Fernández, M., Fried, J.W., García Segura, A.J., Helmling, J., Huber, A., Ibáñez Mengual, J.M., Laun, W., Lenzen, R., Rodríguez Gómez, J.R., and Rohloff, R., “Characterization and Performance of the 4k x 4k Hawaii-2RG Mosaic for PANIC”, Proc. SPIE 7742 , 77421R (2010)

[6] Storz, C., Naranjo, V., Mall, U., Ramos, J., Bizenberger, P., and Panduro, J., “Standard modes of MPIA's current H2/H2RG-readout systems”, Proc. SPIE 8453, 84532E (2012)

[7] Blank, R., Anglin, S., Beletic, J. W., Bhargava, S., Bradley, R., Cabelli, C. A., Chen, J., Cooper, D., Demers, R., Eads, M., Farris, M., Lavelle, W., Luppino, G., Moore, E., Piquette, E., Ricardo, R., Xu, M., and Zandian, M., "H2RG focal plane array and camera performance update", Proc. SPIE 8453, 845310 (2012)

[8] Stahle, C., Hill, B., Babu, S., Blake, P., Beletic, J. W., Cleveland, K., Jhabvala, C., Greenhouse, M., Kimble, R., Kopp, R., Lee, C., Leidecker, H., McMurray, B., Pipher, J., Piquette, E., Pontius, J., Rauscher, B. J., Rieke, M., Tennant, B., Wang, L., and Zandian, M., "JWST Detector Degradation Failure Review Board Executive Summary: Root Cause Determination", JWST-RPT-017457 (2011)